Jürgen Fuhrmann

Mathematical and numerical modeling of flow, transport, and reactions in porous structures of electrochemical devices

Abstract: Due to the large surface-to-volume ratio of the reactive interface between the porous matrix and the electrolyte contained in the pore space, porous electrode structures are used in many electrochemical devices including fuel cells, batteries and supercapacitors. The present chapter gives an overview on important aspects of their modeling. Among the different options to derive discrete models, the paper focuses on the Voronoi-box-based finite volume method which allows one to preserve important qualitative physical properties of the continuous problem in the process of discretization.

Keywords: Models of Electrochemical System, Porous Electrode Theory, Finite Volume Method.

Mathematics Subject Classifications 2010: 76V05, 76D05, 65N08, 65N30

Jürgen Fuhrmann: Weierstrass Institute for Applied Analysis and Stochastics, Berlin, Germany, juergen.fuhrmann@wias-berlin.de

1 Introduction

Macroscopic modeling of electrochemical cells allows one to improve the understanding of the interactions between the various coupled transport and reaction processes. It allows the formulation of hypotheses that can be verified in experiments.

Electrochemical reactions typically proceed as electron transfer reactions at the interface between electrodes – electron conducting solids – and electrolytes – ion conducting fluids or solids. Consequently, the overall reaction rate in an electrochemical system scales with the surface area of the electrode. At the same time, this reaction rate is proportional to the current flowing through a whole electrochemical cell. In comparison to flat surfaces electrodes, porous electrodes allow for a larger ratio between electrode surface and device volume. Therefore, porous electrode structures are essential for the optimization of the per volume performance of electrochemical energy conversion devices like fuel cells, batteries, and supercapacitors.

This chapter attempts to review important aspects of the current state-of-the-art in modeling porous electrodes. At the same time, it points at limitations in the current understanding asking for further research. Additionally, it highlights some aspects of the Voronoi-box-based finite volume method which can be used as a versatile tool to derive discrete models of electrochemical systems which can be solved on computers.

1.1 Model scales

In porous electrodes, one can distinguish a number of possibly overlapping spatial scales. These are

- the molecular scale of single ions, electrons, and surface sites;
- the polarization mesoscale, at which charge separation (polarization) between positive and negative charge carriers is observed;
- the electroneutrality mesoscale resolving single pores and allowing to assume electroneutrality;
- the macroscale of the porous electrode with average properties (e.g. similar to Darcy's law in porous media).

It is generally understood that theories connecting the molecular scale with the larger scales are still far from being settled, for a recent attempt of bridge building, see e.g. [62].

This chapter focuses on the mesoscale(s) of the porous space and the macroscale of the electrode.

1.2 The direct methanol fuel cell – an example of an electrochemical device with a porous electrode

An example of a porous electrode can be found in the reaction zones of a direct methanol fuel cell as shown in Figure 5.1. The reaction zones in both the anodic and cathodic sections of such a fuel cell bring into contact several phases:

- reactants and reaction products dissolved in water: for the anode, these are methanol resp. CO_2 and water, for the cathode, these are oxygen and water;
- electrons in the porous matrix of the electrode consisting of carbon paper: this conducting phase has to facilitate the conduction of the electrical current;
- protons in the proton conducting polymer membrane which separates the reaction of methanol combustion into an anodic and a cathodic part;
- catalyst particles facilitating the electrochemical reactions.

An attempt to create a comprehensive macroscopic mathematical and numerical model of the membrane–electrode assembly of such a cell has been performed in [17]. Many elements of this model have been derived based on well-known heuristic ansatzes. For an example of a recent attempt to improve the situation, see, e.g. [81].

The "porous electrode theory" as it is known, e.g. in [68] considers the coupling between the levels of the electrostatic potential in a porous matrix – the carbon paper structure in the example – and in an electrolyte – the polymer membrane in the example. This coupling, together with a number of other processes is a constituting element of the model in [17] as well as of many other models of electrochemical devices. The present chapter attempts to trace the origin of this model and highlights questions concerning its mathematical foundation. A further focus is the nu-

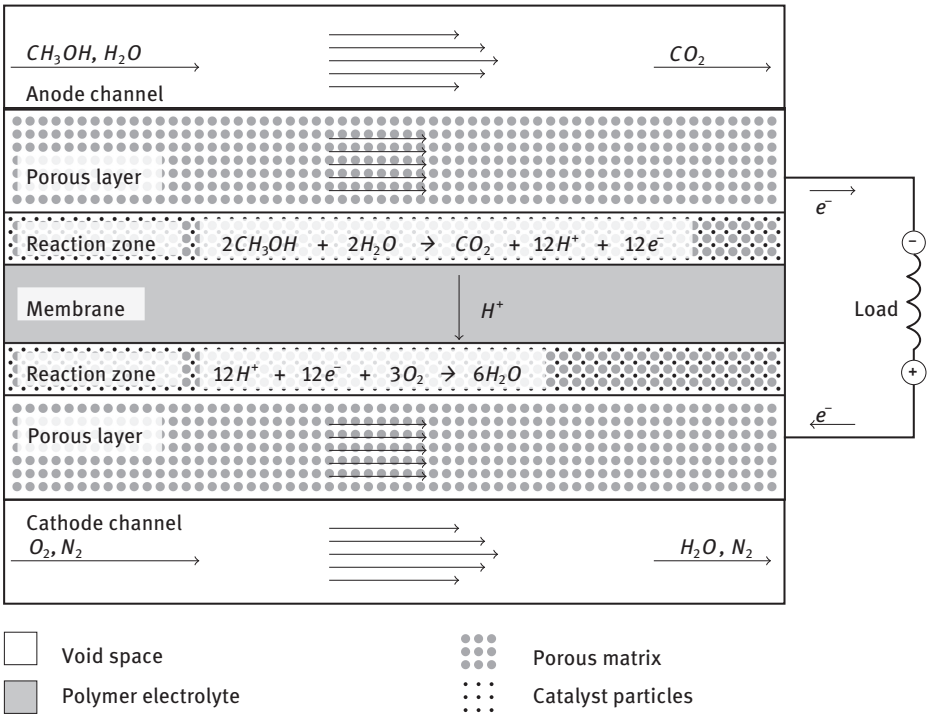

Figure 5.1: Schematic of a direct methanol fuel cell.

merical implementation of the model using the two-point flux Voronoi finite volume method.

2 Electrolytes and interfaces

This section gives a short overview on ion transport in electrolytes as it takes place in the pore space. This discussion at a large extent is inspired by [67].

2.1 Dilute electrolytes

A dilute solution in a spatial domain Ω is a mixture characterized by the existence of a solvent – a species whose fraction in the mixture is significantly larger than that of all other (dissolved) species – in this mixture. In this case it can be assumed that the velocity of the mixture coincides with the velocity of the solvent, and that the discussion of the momentum transport can be decoupled from the discussion of the motion of the dissolved species relative to the velocity of the mixture. Consequently, one as-

sumes a given velocity field of the solvent $\vec{v}$. Another simplification in the ansatz discussed here consists in ignoring the momentum exchange between different dissolved species. For modeling approaches in a more general case see, e.g. [19, 75].

Given an electric field as the gradient of the electrostatic potential ϕ, one identifies three driving forces for the transport of $n+1$ charged (ionic) dissolved species characterized by their concentrations c_i $(i = 0, \dots, n)$ in a spatial domain Ω:

$$\vec{N}_i = -\overbrace{z_i \mu_i F c_i \nabla \phi}^{\text{electromigration}} - \overbrace{D_i \nabla c_i}^{\text{diffusion}} + \overbrace{c_i \vec{v}}^{\text{advection}} \qquad i = 0, \dots, n\,. \tag{5.1a}$$

Here, μ_i is the mobility, D_i the molecular diffusion coefficient, and z_i the charge number of species i. For neutral species, the charge number z_i is zero, for positively charged ions (cations) it is a positive integer, and for negatively charged ions (anions) it is a negative integer. $F = 96\,485.3415\,\mathrm{A\,s/mol}$ is the Faraday constant. Mobility and diffusion coefficient are linked through the Einstein relation $D_i = kT\mu_i$, where $k = 1.381 \times 10^{-23}\,\mathrm{J/K}$ is the Boltzmann constant and T the absolute temperature. This *Nernst–Planck equation* is combined with the continuity equations

$$\partial_t c_i + \nabla \cdot \vec{N}_i = 0 \quad i = 0, \dots, n\,, \tag{5.1b}$$

which assume that no reactions between ionic species take place in the interior of the domain Ω under consideration, taking into account that electrochemical reactions are constrained to interfaces between phases. As one recognizes, in addition to diffusion and convection, charged species move due to the force exerted on them by the electric field $\vec{E} = \nabla\phi$. At the same time the charge distribution influences the electric field via the Poisson equation

$$-\nabla \cdot \varepsilon \nabla \phi = F \sum_{i=0}^{n} z_i c_i\,, \tag{5.1c}$$

where the electric permittivity $\varepsilon = \varepsilon_r \varepsilon_0$ is the product of the relative permittivity of the medium and the vacuum electric permittivity $\varepsilon_0 = 8.85 \times 10^{-12}\,\mathrm{A\,s/V\,m}$. The *Nernst–Planck–Poisson system* (5.1a)–(5.1c) then describes the motion of $n+1$ charged species in the self-consistent electrical field.

The fluid velocity is determined by the Navier–Stokes equations for a fluid of viscosity η with an additional body force due to charge separation

$$\partial_t \vec{v} + (\vec{v} \cdot \nabla)\vec{v} + \nabla p - \eta \Delta \vec{v} = \sum_{i=0}^{n} z_i c_i \nabla \phi, \quad \nabla \cdot \vec{v} = 0\,. \tag{5.2}$$

Analytical investigations for the fully coupled system can be found, e.g. in [75] and [79].

The van Roosbroeck system for charge transport in semiconductor devices can be derived from the Nernst–Planck–Poisson system (5.1a)–(5.1c) for the case $\vec{v} = 0$.

The mobile charged species in this case are the electrons in the conduction band and the corresponding vacancies in the valence band denoted as "holes." A bulk reaction term describing generation and recombination of electron–hole pairs is added. Additional immobile charge carriers are used to describe doping. With Dirichlet, Neumann, or Robin boundary conditions, it is possible to show global existence and uniqueness results [26, 34, 35]. Existence results for the case of more than two species describing dopant diffusion in semiconductors can be found in [37].

2.2 Bulk electroneutrality

If the domain considered is large, due to the fact that $\varepsilon \ll F$, in the interior of the domain, outside a small boundary layer of width λ_D/L, electroneutrality can be assumed

$$\sum_{i=0}^{n} z_i c_i = 0\,. \tag{5.3}$$

Here, L is a characteristic length of the domain (e.g. pore width), and λ_D is the *Debye length* which for a symmetric $z:z$ electrolyte[1] is defined as

$$\lambda_D = \sqrt{\frac{\varepsilon kT}{2z^2e^2C_b}}\,,$$

where $e = 1.602 \times 10^{-19}\,\mathrm{A\,s}$ is the elementary charge, and C_b is a characteristic bulk solute concentration [7]. In aqueous solutions, the Debye length λ_D has a typical range between 1 and 100 nm.

Inside the boundary layer, equation (5.3) is violated, and the resulting space charge influences the distribution of the electrostatic potential. Therefore for moderate sizes of the electric field, the domain containing the electrolyte can be subdivided into a space charge region, where charge separation takes place and a region where electroneutrality holds [76].

In the sequel, some consequences of local electroneutrality are discussed. Summing up the species transport equations multiplied by z_i, respectively, yields

$$\partial_t \left(\sum_{i=0}^{n} z_i c_i \right) - \nabla \cdot \left(\sum_{i=0}^{n} z_i^2 \mu_i F c_i \nabla \phi + \sum_{i=0}^{n} z_i D_i \nabla c_i - \vec{v} \sum_{i=0}^{n} z_i c_i \right) = 0\,. \tag{5.4}$$

1 Electrolyte with two charged species with charge numbers z and $-z$ and equal diffusion coefficients.

The electroneutrality condition (5.3) allows one to express e.g. c_0 through the concentrations of the other species:

$$z_0 D_0 c_0 = -\sum_{i=1}^{n} D_0 z_i c_i \,.$$

Consequently,

$$\nabla \cdot \left(\sum_{i=0}^{n} F z_i^2 \mu_i c_i \nabla \phi + \sum_{i=1}^{n} z_i (D_i - D_0) \nabla c_i \right) = 0 \,,$$

and finally,

$$-\nabla \cdot \sigma \nabla \phi = \nabla \cdot \sum_{i=1}^{n} z_i (D_i - D_0) \nabla c_i \,, \tag{5.5}$$

where $\sigma = F \sum_{i=0}^{n} z_i^2 \mu_i c_i$ is called conductivity.

Equation (5.5) is equivalent to Ohm's law that describes the proportionality of the current to a voltage difference. Under electroneutrality (equation (5.3)), this is now the equation which defines the electrostatic potential. It is formally similar to the Poisson equation (5.1c). However, its physical background is different. Under the circumstances of equal diffusion coefficients, small diffusion coefficients or small concentration gradients, the right-hand side of equation (5.5) can be neglected.

Together with equation (5.1a) (for $i = 1, \ldots, n$), it again describes the motion of $n + 1$ charged species in their self-consistent electrical field under the condition of electroneutrality. The concentration c_0 can be obtained from the electroneutrality condition (5.3).

In the sequel, several examples are discussed which use the electroneutrally condition. The corresponding models are commonly used as building blocks of more complex models.

Example 5.1 (Solid-state conductor)**.** One assumes that a solid-state conductor contains two species, the immobile "lattice" sites with constant concentration c_1 and charge number z_1, and mobile charge carriers with concentration c_0 and charge number $z_0 = -z_1$. One can assume that $\vec{v} = 0$. Furthermore, immobility implies $\mu_1 = D_1 = 0$. Electroneutrality then implies that $c_0 = c_1$ is constant. With $\sigma = z_0^2 \mu_0 F c_0$, charge transport and potential distribution under electroneutrality is completely described by Ohm's law

$$-\nabla \cdot \sigma \nabla \phi = 0 \,.$$

This approach is classically used to describe current distribution in electronic conductors, like graphite or metals, where the mobile charge carriers are electrons.

Likewise, the conduction mechanism in proton conducting polymer membranes assumes the presence of acid groups attached to a polymer membrane keeping negative charges fixed and allowing protons to dissociate from them in the presence of

water taken up by the membrane. Therefore, a similar macroscopic description as in the case of electronic conductors is justified. One however has to note that the amount of mobile protons is proportional to the level of dissociation of the acid groups, which in turn strongly depends on the amount of water available in the membrane, leading to a dependency of the conductivity σ on water content of the membrane [73, 91].

The model ansatz from this example is used for electrons and protons in methanol and hydrogen fuel cell models [17, 52, 73].

Example 5.2 (Carrier electrolyte)**.** Electrochemical experimentation relies on the use of carrier electrolytes. For example, the electrochemical oxidation of hydrogen dissolved in water at platinum electrodes is investigated using H_2SO_4 as a background electrolyte with a concentration much larger than the concentration of the reactant. The hydrogen redox reaction at the electrode results in the production or consumption of protons in an amount so small (but measurable by the electric current from the electrons involved) that the proton concentration in the electrolyte is essentially constant. Once again this leads to the fact that charge transport is facilitated by species with constant concentration, reducing ionic transport to Ohm's law. This assumption is behind many models of potential distribution in electrochemical experimentation [28].

For a sufficiently high concentration of the background electrolyte, the conductivity σ can be assumed to be high. Then, depending on the geometry of the device, and the position of the counter electrode, in the bulk, the potential is nearly constant, and Ohm's law can be dropped from the consideration altogether. As a result, only the electroneutral species has to be considered in modeling. Classically, this setting has been used for rotating disk electrodes [57], and recently in the interpretation of flow cell experiments [31, 33].

Example 5.3 (Symmetric electrolyte)**.** An important example that is useful in the development of many theoretical concepts is the symmetric $1:1$ electrolyte, where only two charged species exist with charge numbers $z_0 = 1$ and $z_1 = -1$ and the assumption $D_0 = D_1 = D$. In that case, the bulk electroneutrality condition allows one to write $c_0 = c_1 = c$, and the charge transport under these conditions is described by the pair of equations

$$-\nabla \cdot \sigma \nabla \phi = 0 \tag{5.6}$$

$$\partial_t c - \nabla \cdot (D \nabla c - c\vec{v}) = 0\,. \tag{5.7}$$

In this case, in the bulk, the electrolyte concentration is not influenced by the electric field. The electrostatic potential can influence the species concentration via boundary conditions involving reactions.

2.3 Double layer

The assumption of bulk electroneutrality leads to the fact that deviations from electroneutrality happen in a thin boundary layer at the interface between different electrolyte materials. A prominent example of this situation is the interface between an electrode consisting of an electronic conductor and an electrolyte. If there is no reaction at the interface (ideally polarizable electrode), then nevertheless, charge may accumulate around the interface: if the electrode is charged, within the electrolyte, positively charged ions accumulate near the interface, see Figure 5.2. Moreover, other adsorption-like processes due to the polarity of ions can lead to the accumulation of charge directly at the surface (inner Helmholtz layer) and, for solvated ions, close to the surface (outer Helmholtz layer).

With certain limitations, this charge accumulation can be described using the Nernst–Planck–Poisson system. As the relaxation time in the boundary layer is small in comparison to the other timescales changing the system, it can be assumed that the boundary layer is in thermodynamic equilibrium. In this case, $\vec{N}_i = 0$, and the Nernst–Planck equation allows to express

$$c_i = c_i(\phi) = c_{i,b} \exp\left(\frac{e}{kT} z_i \phi\right) , \tag{5.8}$$

where $c_{i,b}$ is the bulk concentration, transforming the Nernst–Planck–Poisson system into the Poisson–Boltzmann equation

$$-\nabla \cdot \varepsilon \nabla \phi = F \sum_{i=0}^{n} z_i c_{i,b} \exp\left(\frac{e}{kT} z_i \phi\right) .$$

This equation can be regarded in the one-dimensional domain $(0, \infty)$ with boundary conditions $\phi|_{x=0} = \phi_s$, where ϕ_s is the applied electrode potential, and $\phi|_\infty = \phi_b$. The resulting unique solution $\phi(x)$ can be used to calculate the stored charge

$$Q_{dl} = Q_{dl}(\phi_s - \phi_b) = \int_0^\infty F \sum_{i=0}^{n} z_i c_i(\phi) dx .$$

This value gives an estimate of the charge in the boundary layer depending on the potential difference between bulk and electrode, and the bulk electrolyte concentration.

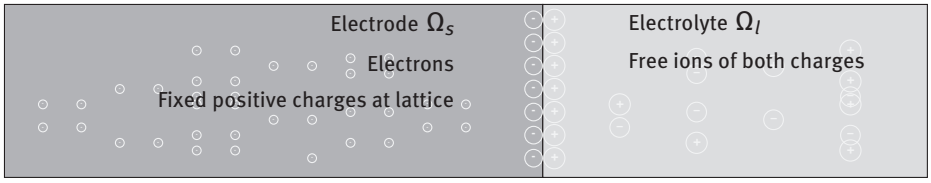

Figure 5.2: Sketch of interface between electrode and electrolyte with charge accumulation.

One notes that the charge stored outside the boundary layer in the domain (λ_D, ∞) is only marginal. This estimate lies on the base of the Gouy–Chapman theory [6, 7] which can be seen as valid for small potential differences. The main drawback of this approach is the fact that behind the formulation of the Nernst–Planck equation as introduced here, stands an exponential dependency of the species concentration on its electrochemical potential, as seen in equation (5.8). This Boltzmann-type exponential dependency assumes that charged particles are ideal point charges and thus ignores that the species concentrations must be limited by the finite particle size.

A widespread approach adds an additional layer of solvated ions with zero charge density (Stern layer) at the electrode surface, resulting in better representation of experimental data. Other more recent approaches attempt to use improved models for the dependency of species concentration on the electrochemical potential [19, 21, 54]. In order to be consistent, it would be necessary to incorporate these into Nernst–Planck flux expression (equation (5.1a)) which lies outside of the scope of this chapter.

Under the assumption of electroneutrality, the double-layer charge model allows one to approximate the charge in the boundary layer by a surface charge expression at the electrode–electrolyte boundary Γ_{ls}:

$$-\nabla \cdot \sigma \nabla \phi = 0 \qquad \text{in } \Omega_l \tag{5.9}$$

$$\sigma \nabla \phi \cdot \vec{n} = \partial_t Q_{dl} \quad \text{on } \Gamma_{ls}\,. \tag{5.10}$$

This boundary condition is nonlinear due to the potential dependency of Q_{dl} and describes the charge resp. discharge of the double layer as a current sink resp. source. Together with the Nernst–Planck equation for species $1, \ldots, n$ and appropriate reaction boundary conditions for these concentrations, one might refer to equation (5.9) as the thin double-layer limit of the Nernst–Planck–Poisson system.

A widespread way to model the double-layer charge introduces the differential double-layer capacitance $C_{dl} = \frac{dQ_{dl}}{d\xi}$ and assumes a linear dependency

$$Q_{dl} \approx C_{dl}(\phi - \phi_s)\,,$$

where ϕ_s is the value of the applied potential. The assumption of a constant double-layer capacitance often is made for simplicity, but holds only under narrow conditions. In general, this capacitance again depends on the voltage drop, and on the electrolyte concentration. In [11], a nonlinear expression derived from Gouy–Chapman theory [7] is introduced into porous electrode theory instead of a constant double-layer capacitance.

Matched asymptotic expressions have been used to provide a stronger mathematical background to the separation of the electrolyte into a double layer in electrostatic equilibrium and an electroneutral bulk in the thin double-layer limit [76].

2.4 Interface between electrode and electrolyte

For sufficiently large system dimensions, at the ideally polarizable interface between electrode and electrolyte, conduction processes on both sides of the interface Γ_{ls} can be described in the thin double-layer limit. The coupling of the potential between the two phases is mediated by an interface condition based on the double-layer model:

$$-\nabla \cdot \sigma_l \nabla \phi_l = 0 \qquad \text{in } \Omega_l \tag{5.11}$$

$$-\nabla \cdot \sigma_s \nabla \phi_s = 0 \qquad \text{in } \Omega_s \tag{5.12}$$

$$\sigma_l \nabla \phi_l \cdot \vec{n} = \partial_t C_{dl}(\phi_l - \phi_s) \qquad \text{on } \Gamma_{ls} \tag{5.13}$$

$$-\sigma_s \nabla \phi_s \cdot \vec{n} = \partial_t C_{dl}(\phi_l - \phi_s) \qquad \text{on } \Gamma_{ls}\,. \tag{5.14}$$

Here ϕ_s and ϕ_l refer to the electrostatic potential in the electrode domain Ω_s and electrolyte domain Ω_l, respectively. Instead of a thin transition layer between the respective bulk potential values, based on the thin double-layer limit assumption, a potential jump is assumed which results in two different levels of the electrostatic potential.

2.5 Faradaic reactions

Electrochemical reactions involve electron transfer, and thus they take place at the interface between an electrolyte and a conductor. The Butler–Volmer model relates the rate of such a reaction to the potential jump at the interface. For a typical electron transfer reaction of the kind

$$A + e^- \rightleftharpoons B\,,$$

the rate expression reads as

$$j = k^+ c_A e^{(1-\alpha)F\frac{\Delta\phi}{RT}} - k^- c_B e^{\alpha F \frac{\Delta\phi}{RT}}$$

where $\Delta\phi = \phi_l - \phi_s$ [4].

In the presence of a Faradaic reaction, a second source/sink term according to the creation of charge occurs in the potential coupling at the interface, and the interface conditions in equations (5.13) and (5.14) have to be updated:

$$\sigma_s \nabla \phi_s \cdot \vec{n} = \partial_t (C_{dl}(\phi_l - \phi_s)) + jF \qquad \text{on } \Gamma_{ls}$$

$$-\sigma_l \nabla \phi_l \cdot \vec{n} = \partial_t (\partial_t C_{dl}(\phi_l - \phi_s)) + jF \qquad \text{on } \Gamma_{ls}\,.$$

Furthermore, for the species concentrations involved, one arrives at nonlinear boundary conditions of the kind

$$\vec{N}_i \cdot \vec{n} = j \qquad \text{on } \Gamma_{ls}\,. \tag{5.15}$$

The rate expression for a more general reaction

$$\sum_{i=1}^{n} a_i A_i \rightleftharpoons \sum_{i=1}^{n} b_i B_i + ne^- + nH^+$$

generalizes to

$$r = k^+ e^{\frac{n\alpha(\phi_s-\phi_l)F}{RT}} \prod_{i=1}^{n} c_{A_i}^{a_i} - k^- e^{\frac{(1-\alpha)(\phi_s-\phi_l)F}{RT}} \prod_{i=1}^{n} c_{B_i}^{b_i} \tag{5.16}$$

and it has to be added to the boundary conditions as demonstrated in equation (5.15).

3 Porous electrodes

3.1 Ideally polarizable porous matrix

For the discussion of porous electrode models, one may start with the following problem. Assume a porous medium consisting of solid matrix (indexed by s) that consists of an electronic conductor, and a proton conducting polymer electrolyte (indexed by l). First, we assume that the interface between the conductor and the electrolyte in the pore space represents an ideally polarizable electrode, such that no reactions occur at the interface.

At the core of the porous electrode theory lies a model that describes the coupling between the electrostatic potential ϕ_s of the solid matrix and an the electrostatic potential ϕ_l of the electrolyte in the pore space under the assumption that now, they both spread over the porous electrode domain Ω:

$$\partial_t \overline{C}_{dl}(\phi_s - \phi_l) - \nabla \cdot \overline{\sigma}_s \nabla \phi_s = 0 \quad \text{in } \Omega \tag{5.17a}$$

$$\partial_t \overline{C}_{dl}(\phi_l - \phi_s) - \nabla \cdot \overline{\sigma}_l \nabla \phi_l = 0 \quad \text{in } \Omega\,. \tag{5.17b}$$

Here, $\overline{C}_{dl}$ is the volume averaged differential double-layer capacitance, $\overline{\sigma}_s$ is the volume averaged (electronic) conductivity of the matrix, and $\overline{\sigma}_l$ is the volume averaged (ionic) conductivity of the electrolyte in the pore space. Like in a dual porosity model [40], two continua intertwined but spatially separated at the microscale are described by two continua spreading throughout the full space at the macroscale. Heuristic approaches can be used to relate $\overline{\sigma}_s, \overline{\sigma}_l$ to σ_s, σ_l via the porosity of the porous medium, see e.g. [17].

The main assumption that links this model to the electrolyte models in Section 2 is the fact that both within the pore space and the porous matrix, the electroneutrality assumption holds which means that the boundary layers in the porous electrode have to be sufficiently thin in comparison to the pore size.

With respect to electrochemical applications, this model and related ones have been discussed in the survey [68], early papers on this topic appeared around

1960 [22, 51, 69]. The model ansatz has been derived more or less by heuristic considerations and considerations from nonequilibrium thermodynamics [51], without direct derivation from a microstructure model. Nevertheless, this ansatz is the part of a large number of modeling approaches for fuel cells and batteries.

A similar model (where the conductivities are anisotropic due to a genuinely anisotropic microstructure) is the bidomain model used to describe the electrical behavior of cardiac tissue. In this case, equation (5.17a) corresponds to the intercellular potential, and equation (5.17b) corresponds to the channel potential. Cells and channels are separated by membranes which bear additional gating variables. Volume averages of these gating variables enter the macroscopic model as well. The bidomain model goes back to the semiheuristic derivation [64]. A derivation from a pore scale model, based on the thin double layer limit by periodic homogenization, has been undertaken in [49, 66], see also [29]. More modern techniques that go beyond the formal derivation by two-scale asymptotics based on Γ-convergence have been used in [72]. In this case, it is possible to show the convergence of the microscale model to the macroscale model when the characteristic size of the microstructure approaches zero. In effect, the bidomain model then is the result of two consecutive asymptotic limit procedures: first the derivation of the Poisson–Nernst–Planck equations in the thin double layer limit is performed, after that, periodic homogenization results in the macroscopic problem.

In [14], periodic homogenization is used in a similar approach in order to derive a lithium ion battery model which, as a particular feature, includes lithium intercalation into the electrodes.

Another body of work concerns porous media where the porous matrix is an agglomeration of insulating (dielectric) particles, as for example in clays. Consequently, there is no electronic conduction in the porous matrix. All current conducted by a sample has to be attributed to ionic conduction in the electrolyte accumulated in the pore space. However, due to their microstructure, clay minerals may bear a fixed charge which attracts ions, a process which – especially when the ions are solvated – explains swelling processes in porous media. While due to the dielectric properties of the matrix, one cannot speak of a porous electrode, this case is nevertheless worth mentioning because significant results have been obtained by upscaling the Poisson–Nernst–Planck–Stokes system in the pore space using a periodic homogenization approach without the thin double layer assumption [2, 63, 65, 74, 80].

3.2 Species transport

The transport of electroneutral dissolved species in porous electrodes can be modeled according to the same principles as it is done for other porous media [8]. The same is true in the case where the effect of potential gradients is small, as e.g. for symmetric 1 : 1 electrolytes assuming thin double layers in comparison to the pore size.

Homogenization in the case of a porous matrix consisting of insulating charged particles with fixed charge has led to a macroscopic Poisson–Nernst–Planck system [65, 74, 80].

3.3 Darcy flow

As in the pore space the flow velocity can be assumed to follow the Stokes resp. Navier–Stokes equations, the use of Darcy's equation on the macroscale is a justified [8, 45] if the porous electrode is fully saturated. One however has to take into account the fact that a flow proportional to the amount of moving ions is induced due to the electroosmotic drag effect [92] which describes the motion of fluid molecules in the solvatization hull of ions as another transport mechanism for fluid molecules:

$$\vec{v} = k\nabla p + \sum_{i=0}^{n} \delta_i z_i \vec{N}_i \quad \nabla \cdot \vec{v} = 0\,. \tag{5.18}$$

The drag coefficients δ_i describe the amount of fluid carries by an ion of species c_i.

3.4 Further effects

3.4.1 Two-phase flow

Reactants and reaction products in porous electrodes may belong to different phases. In this case, two-phase flow effects have to be taken into account. This situation is typical to low-temperature fuel cells where liquid water and gaseous reactants coexist. A particular difficulty arises from the fact that in these fuel cell electrodes, molecules in different phases have to be moved in different directions. Therefore, the pore space of fuel cell electrodes is modified using, e.g. teflon in order to decrease the wettability for water.

A common heuristic approach in the case of gas/liquid flow assumes a constitutive relationship between capillary pressure and fluid saturation, and saturation dependent relative permeabilities for gases and solvent [43]. In order to describe this situation, methods from two-phase flow modeling in the subsurface have been adopted to the situation in fuel cells [1, 17], sometimes using new ansatzes to express the relationships between capillary pressure and saturation.

Significant efforts are undertaken in order to describe real fuel cell electrodes on the microscale level based on tomographic methods [10].

3.4.2 Gas mixture

The gaseous phase in fuel cell electrodes often consists of multiple species. If the cathode, e.g. is exposed to air, oxygen, and gaseous hydrogen take part in the fuel cell

reaction, while nitrogen is inert. This effect is taken into account by using the Stefan–Maxwell model of flow of a gas mixture in a porous medium which assumes that collision forces between different species molecules balance with the partial pressure gradient. In combination with a two-phase flow model, this modeling approach was used in [17].

3.5 Coupling between porous electrodes and free flow

The Darcy–(Navier)–Stokes coupling, based on the Beavers–Joseph–Saffman boundary conditions [9, 77], appears to be sufficiently well founded, including as successful attempt based on homogenization [48]. Due to compatibility of equation types, the Brinkman equation [13] in several cases is also used [85], though the theoretical justification only includes cases with large pore sizes [59]. A compromise approach includes a thin Brinkman transition layer between Darcy and free flow domain [56].

Significant additional processes have to be taken into account here. These include solute transport through the porous interface, which in a rather plausible way can be modeled based on the continuity of species flux and species concentration.

Far from satisfactory is the modeling of two-phase flow coupling between free flow and porous media flow. While in the Darcy-based two-phase porous media flow model, the coexistence of phases at the microscale allows one to justify an averaging approach leading to the coexistence of the phases on the macroscale, experimentally, one observes droplets [71] resp. bubbles [58] at the macroscale which have to be resolved in proper models. Their existence influences the macroscopic cell performance in significant ways, and, in some cases, is utilized to remove the necessity to use active components for reactant supply resp. product removal [71].

3.5.1 Insertion electrodes

Current lithium-ion batteries are based on insertion electrodes which store atomic lithium. These consist of particles of graphite in the case of the anode, and of $LiCoO_2$, $LiPFeO_4$, or other substances for the cathode. The particles of these materials constitute the porous matrix of these electrodes. Differently from all other porous materials discussed so far in this paper, they allow for the inclusion of lithium atoms into the crystal lattice. Current models assume spherical particles and describe the lithium concentration in the particles depending on the radial position [18, 20].

3.5.2 Precipitation

Precipitation effects in porous electrodes play a significant role in new battery concepts which include rechargeable lithium-air and lithium-sulfur batteries. Here, during discharge, lithium peroxide resp. lithium sulfate in the solid form accumulate in

the pore space of the cathode. During charge, this reaction is reversed, and lithium is stored either in the metallic from or in intercalation electrodes. Current modeling takes these effect into account by a decrease in the porosity dependent on the product content [50, 53].

3.5.3 Temperature effects

Temperature effects can significantly influence the performance of electrochemical devices. Exothermal resp. endothermal interface reactions can be modeled on the macroscopic level by heat sources resp. sinks. Moreover, ion mobilities are temperature dependent, and Joule heat sources due to ion motion can have a significant influence, as discussed, e.g. in [61].

3.5.4 Mechanical effects

Still, more processes are connected with porous electrodes. In particular, insertion electrodes shrink and swell depending on lithium content in the porous matrix [82]. Clays soaking up water swell due to strong electrocapillary forces [63].

4 Numerical approximation by Voronoi finite volumes

Evaluation of electrochemical cell models based on asymptotic approximations is widespread in the electrochemical community [67]. These methods have been developed before the ubiquitous availability of digital computers. Being very successful, they – as well as other analytic modeling approaches [52] – are limited to special cases, simplified models and well-designed experimental situations.

Numerical approximations allow one to solve much more general coupled electrochemical models.

Many interesting effects at electrode/electrolyte interfaces and in porous electrodes can be discussed in a one-dimensional settings, and therefore, finite difference methods are a popular tool for the numerical description of these problems among electrologists, and they remain so up to now [50, 53].

Often, devices have a strongly anisotropic structure, therefore so-called 1 + 1D approaches are used to simplify the geometrical situation [73] and to fall back to finite difference approximations.

Finite element methods provide a well understood and flexible way to discretize coupled models in arbitrary space dimensions. Discontinuous Galerkin methods promise higher flexibility with respect to meshing while keeping the advantage of high-order approximations.

Finite volume methods allow to generalize the finite difference approach to several space dimensions, and at the same time are able to keep the metaphor of the representative elementary volume which is a key element in the derivation of the physical models described here.

This class of methods by itself became rather large. This chapter focuses on the two-point flux Voronoi-box-based finite volume method [60], sometimes referred to simply as the box method [5].

Some other two-point flux finite volume methods use the discretization simplices [25] or the Donald boxes (constructed by joining the centers of mass and the edge midpoints of adjacent simplices) [30] as control volumes. The discrete duality finite volume method [44] has been successfully used for the bidomain model, as it is particularly well suited to approximate the strong anisotropy occurring in the models [12, 16].

4.1 Description of the method

The Voronoi finite volume method based on two-point fluxes needs proper grid alignment in order to approximate anisotropies in a convergent manner [25]. On the other hand, it has the significant advantage that it can – based on well-understood stabilization techniques – guarantee local and global maximum principles and stability in all space dimensions. In the sequel, we give a short overview on this method, related results and its usage.

The models discussed in this paper are systems of N partial differential equations of convection/diffusion/reaction type in a d-dimensional domain with appropriate boundary conditions. For a given velocity d-vector $\vec{v}$, in the interior of the domain, they can be described as

$$\partial_t \mathbf{b}(\vec{x}, \mathbf{u}) + \nabla \cdot \vec{\mathbf{j}}(\vec{x}, \mathbf{u}) + \mathbf{r}(\vec{x}, \mathbf{u}) = 0\,, \tag{5.19}$$

where x is the d-vector of spatial coordinates, $\mathbf{u}(\vec{x}, t) = (u_1(\vec{x}, t), \ldots, u_N(\vec{x}, t))$ is a N-vector valued function describing the unknowns of the problem, $\mathbf{b}(\vec{x}, \mathbf{u}) = (b_1(\vec{x}, \mathbf{u}), \ldots, b_N(\vec{x}, \mathbf{u}))$ is a N-vector valued function of storage terms, $\mathbf{r}(\vec{x}, \mathbf{u}) = (r_1(\vec{x}, \mathbf{u}), \ldots, r_N(\vec{x}, \mathbf{u}))$ is a N-vector valued function of reaction terms, $\vec{\mathbf{j}}(\vec{x}, \vec{v}, \mathbf{u}) = (\vec{j}_1(\vec{x}, \vec{v}, \mathbf{u}), \ldots, \vec{j}_N(\vec{x}, \vec{v}, \mathbf{u}))$ is a $N \times d$-tensor valued function of flux terms. The flux terms are assumed to be the sum of convective and diffusive fluxes. Only some of the species fluxes need to depend on the velocity $\vec{v}$, and one might identify $\vec{v}$ with one of the $\vec{j}_i$, introducing an additional coupling in the system.

In order to describe the discretization approach, assume that the computational domain Ω is subdivided into control volumes $K, L, \ldots$, and that the time interval $[0, T]$ under consideration is subdivided by a partition $0 = t^0 < t^1 < \cdots < t^n = T$. Given a simplicial partition of the domain, one chooses the circumcenter of each simplex and constructs the Voronoi box based on the perpendiculars from the circum-

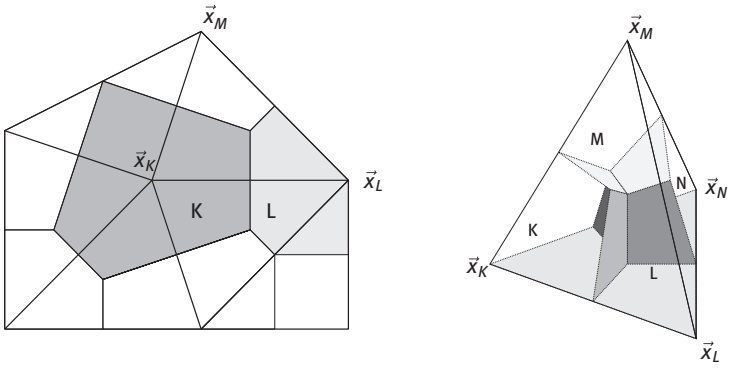

Figure 5.3: 2D and 3D Voronoi construction.

centers to the edges of the corresponding triangle (resp. faces of the corresponding tetrahedron; see Figure 5.3).

If

(1) the interior of the circumsphere of any simplex does not contain any simplex node;
(2) and all simplex circumcenters belong to the closure of the domain Ω.

then this construction is justified and results in well-defined control volumes with the property that their boundaries consist of straight resp. planar parts which are orthogonal to the corresponding simplex edges. The two conditions define the boundary conforming Delaunay property of the simplicial partition and need to be ensured in the mesh generation process [83, 84, 86, 88]. The resulting control volume mesh is admissible in the sense of the convergence theory developed in [25].

For each space-time control volume $K \times (t^{n-1}, t^n)$, one integrates equation (5.19) and divides by the time difference:

$$0 = \frac{1}{t^n - t^{n-1}} \int_{t^{n-1}}^{t^n} \int_K \left(\partial_t \mathbf{b}(\vec{x}, \mathbf{u}) + \nabla \cdot \vec{\mathbf{j}}(\vec{x}, \mathbf{u}) + \mathbf{r}(\vec{x}, \mathbf{u}) \right) dx dt \,. \tag{5.20}$$

Application of the Gauss theorem to the integral of the flux divergence, choosing a quadrature in space which is centered at the Voronoi box center $\vec{x}_K$ and choosing a quadrature in time which yields an implicit scheme leads to

$$0 = |K| \left(\frac{\mathbf{b}(\vec{x}_K, \mathbf{u}_K^n) - \mathbf{b}(\vec{x}_K, \mathbf{u}_K^{n-1})}{t^n - t^{n-1}} + \mathbf{r}(\vec{x}_K, \mathbf{u}_K^n) \right) - \int_{\partial K} \vec{\mathbf{j}}(\vec{x}, \vec{v}, \mathbf{u}^n) \cdot \vec{n} ds \,. \tag{5.21}$$

Splitting the surface integral into contributions from the facets common with the neighboring control volumes $L \in \mathcal{N}(K)$, applying quadrature rules, and introducing the flux function $\mathbf{g}(\mathbf{u}_K^n, \mathbf{u}_L^n, v_{KL})$ to approximate the scaled normal flux $\vec{\mathbf{j}}(\vec{x}, \mathbf{u}) \cdot$

$(\mathbf{x}_K - \mathbf{x}_L)$ through a common facet $\sigma_{KL} = \partial K \cap \partial L$ yields

$$0 = |K| \left(\frac{\mathbf{b}(\vec{x}_K, \mathbf{u}_K^n) - \mathbf{b}(\vec{x}_K, \mathbf{u}_K^{n-1})}{t^n - t^{n-1}} + \mathbf{r}(\vec{x}_K, \mathbf{u}_K^n) \right) - \sum_{L \text{ nb. of } K} \frac{|\partial K \cap \partial L|}{|\vec{x}_K - \vec{x}_L|} \mathbf{g}(\mathbf{u}_K^n, \mathbf{u}_L^n, v_{KL}) \,. \quad (5.22)$$

Here, v_{KL} is a projection of the velocity field $\vec{v}$ on to the simplex edge $\vec{x}_K\vec{x}_L$. The last step took advantage of the fact that the simplex edge joining the centers $\vec{x}_K, \vec{x}_L$ of neighboring Voronoi boxes K, L is perpendicular to the common face $\partial K \cap \partial L$. Thus, a finite difference flux expression in the unknowns u_K, u_L in a natural way approximates the normal flux $\vec{j} \cdot \vec{n}_{KL}$.

4.2 Flux expressions for scalar convection diffusion

Convection–diffusion problems are the main building blocks of the models under consideration.

Example 5.4. For a scalar, linear diffusion problem, one has $j = D\nabla u$, and one would choose $g(u_K, u_L) = D(u_K - u_L)$ as flux expression. For this case, the method dates back to [60]. This method falls in the class of finite volume methods whose convergence is covered by the theory in [25].

Example 5.5. A scalar, linear convection diffusion flux in a given continuous velocity field $\vec{v}(\vec{x})$ is described as

$$j = D\nabla u + u\vec{v}(\vec{x}) \,.$$

The value

$$v_{KL} = \frac{1}{|\partial K \cap \partial L|} \int_{\partial K \cap \partial L} \vec{v}(s) \cdot (\vec{x}_K - \vec{x}_L) ds \quad (5.23)$$

defines an averaged projection of the velocity field $\vec{v}$ onto the scaled control volume normal $\vec{x}_K\vec{x}_L$. Using this value, it is possible to formulate an upwind flux expression

$$g(u_K, u_L, v_{KL}) := D \left(U\left(\frac{v_{KL}}{D}\right) u_K - U\left(-\frac{v_{KL}}{D}\right) u_L \right) . \quad (5.24)$$

There are several choices for the upwind function U. For

$$U(\xi) = \begin{cases} 1 + \xi & \xi \geq 0 \\ 1 & \xi < 0 \,, \end{cases}$$

one obtains the simple upwind scheme covered by the theory in [25]. In the case of a H^2 regular solution, one obtains $O(h)$ convergence in a discrete H^1-norm and the L^2-norm [38]. Per time step, this approach yields a linear system of equations

$\mathbf{B}u^n + \mathbf{A}u^n = \mathbf{B}u^{n-1}$ with a positive diagonal matrix $\mathbf{B}$. The graph of the matrix $\mathbf{A}$ is connected, $\mathbf{A}$ has column sum zero, nonpositive off-diagonal entries and nonnegative main diagonal entries. As a consequence, $\mathbf{I} + \mathbf{B}^{-1}\mathbf{A}$ has the M-property [90]. Therefore, $u^{n-1} \geq 0$ implies $u^n \geq 0$. Furthermore, the scheme obeys a discrete maximum principle which prevents any nonphysical oscillations.

Example 5.6. If in equation (5.24), one chooses the Bernoulli function $U(\xi) = B(\xi) = \frac{\xi}{e^{-\xi}-1}$, one obtains the exponential fitting scheme independently introduced by [3, 47, 78]. In addition to the advantageous properties of the upwind scheme of Example 5.5, this ansatz minimizes the artificial diffusion introduced to guarantee the stability of the scheme, in some cases leading to improved convergence rates [55].

In the case of a Nernst–Planck equation with zero solvent velocity, one relates $\vec{v} = \nabla\phi$ to the gradient of the electrostatic potential and $v_{KL} = (\phi_K - \phi_L)$ to its discrete analog. The resulting coupled electroreaction–diffusion equations have been handled, e.g. in [41]. In particular, [36] contains a proof of the dissipativity of the scheme, adding another qualitative property which is conserved during the discretization process by Voronoi finite volumes.

Example 5.7. In [78], the exponential fitting scheme of Example 5.6 has been derived by gluing together local solutions along the edges $\vec{x}_K\vec{x}_L$.

For a scalar, nonlinear convection diffusion flux is given by

$$j = D(u)\nabla u + F(u)\vec{v}(\vec{x}),$$

one can generalize this approach by defining $g(u_K, u_L, v_{KL}) := G$ from the solution of a local Dirichlet problem for the projection of the nonlinear equation onto the edge $\vec{x}_K\vec{x}_L$ [23]: Let $w(\xi) := u(\vec{x}_L + \xi(\vec{x}_K - \vec{x}_L))$ such that

$$\begin{cases} D(w)w' + F(w)v_{KL} = G \\ w(0) = u_L \\ w(1) = u_K\,. \end{cases}$$

4.3 Coupling to flow problems

Both the Navier–Stokes equations and the Darcy equation result in a divergence free velocity field ($\nabla \cdot \vec{v} = 0$). For a scalar convection diffusion problem, this condition results in the continuous maximum principle for the concentration of a transported species: in the absence of volume sinks and sources, the solution in a given point $\vec{x}$ is bounded by its values in a neighborhood of $\vec{x}$.

The discrete counterpart of this condition involves the velocity projection v_{KL}:

$$\sum_{L \text{ nb. of } K} \frac{|\partial L \cap \partial K|}{|\vec{x}_K - \vec{x}_L|} v_{KL} = 0\,. \tag{5.25}$$

If this condition is fulfilled, the discrete maximum principle is valid: the discrete solution in point x_K is bounded by its values in neighboring points x_L [23, 32].

Example 5.8. A pointwise divergence free velocity field $\vec{v}(\vec{x})$ leads to equation (5.25) when v_{KL} is obtained by exact calculation of the integral in equation (5.23). This in appropriate physical situations allows one to use known analytical expressions (Hagen Poiseuille [31] and von Karman–Cochran [57]) for the velocity field $\vec{v}(\vec{x})$.

Pointwise divergence free finite elements provide another option to ensure equation (5.25). A particular choice is the lowest order Scott Vogelius element for the Navier–Stokes equations. This element is based on ansatz spaces of continuous, piecewise polynomial vector functions of order d for the velocity and discontinuous, piecewise polynomial functions of order $d-1$ for the pressure. This combination is LBB-stable on certain macro triangulations. The convergence of the coupled finite-element finite-volume method for the stationary Navier–Stokes equation coupled to the transport of a dissolved electroneutral species has been proven in [32], and applied to a thin layer electrochemical flow cell problem in [33].

Example 5.9. The Voronoi finite volume scheme for the Darcy flow problem (equation (5.18)) directly leads to the discrete divergence condition. In this case $\vec{v} = \vec{j} = K\nabla p$, and correspondingly, one chooses $v_{KL} = g(p_K, p_L) = K(p_K - p_L)$ which automatically fulfills equation (5.25).

Example 5.10. While the coupling in the case of divergence free finite elements as described in Example 5.8 provides the desired maximum principle, in particular due to the large number of finite element degrees of freedom it is expensive.

It would be desirable to obtain a finite volume discretization of the Navier–Stokes equations which directly leads to equation (5.25), very much like in Example 5.9.

A compatible finite volume scheme based on the approach of [70] generalizing the MAC scheme [42] is currently under investigation [24]. This method involves pressure unknowns p_K in the simplex mesh nodes and velocity unknowns v_{KL} in the direction of the simplex mesh edges. The divergence equation is exactly equation (5.25).

4.4 Software

The Voronoi finite volume method is a rather versatile tool in the description of coupled problems. The toolbox pdelib [89] implements an API which allows for a straightforward implementation of the discretization method for the problem class as in equation (5.19). In order to specify a particular problem, a user has to provide the discretization grid and the functions $\mathbf{b}(\vec{x}_K, \mathbf{u}_K)$, $\mathbf{r}(\vec{x}_K, \mathbf{u}_K)$, $\mathbf{g}(\mathbf{u}_K, \mathbf{u}_L, v_{KL})$ along with the partial derivatives with respect to $\mathbf{u}_K, \mathbf{u}_L$. Based on these data, the software implements Newton's method to solve equation (5.22). The size of the time steps can be chosen in an adaptive manner, it is possible to choose among a number of direct

and iterative methods to solve the linear systems of equations arising from Newton's method. It incorporates the mesh generators triangle [84] and TetGen [86]. It is possible to vary the sets of equations and species between different subdomains of the computational domain. The code has been parallelized for multicore computers using OpenMP directives and based on a proper grid partitioning. For the convenience of the user it contains OpenGL-based online graphics, user interfaces can be built using the Lua scripting language [46] and the FLTK toolkit [15].

5 Conclusions

Porous electrodes in electrochemical devices are a rich source of mathematical and numerical problems with significant relevance to applications. A large part of the models used are based on well-founded heuristics together with experimental comparison. Rigorous upscaling from pore level to the macroscopic level taking into account the electrical effects has been performed in several interesting cases, but still does not cover many significant application cases.

At the same time, it seems to be reasonable to investigate these problems using detailed numerical simulations on the pore scale.

The heuristic approach used in this chapter to describe the current models in usage ignored the fact that at the macroscopic level, thermodynamic thinking is available that allows one to add an additional level of consistency to the models. In particular, instead of concentrations, chemical potentials can be used, and not always in this context, Boltzmann statistics links chemical potential with concentrations [19, 54]. Corresponding modifications may help to improve the double layer models cited. The preservation of thermodynamical correctness at the discrete level is another point of interest. Due to its properties, the Voronoi finite volume method is a good candidate for a discretization scheme delivering these properties.

Understanding from the molecular scale is needed in order to improve understanding of the processes at electrode surfaces. In particular, data like activation energies could be available from density functional theory. On the other hand, methods for upscaling of full kinetic data from the microscale are in a very early stage of development [62].

Concerning the implementation of numerical methods based on the models described, the paper focused on the Voronoi finite volume method. In this context, the method has several advantages. It focuses on the conservation character of mathematical model allowing to see the discretized partial differential equation as discrete problem of its own merit. Electrochemists often think in equivalent circuits, and the method is mathematically equivalent, moreover, it arose from this way of thinking [60]. It allows the straightforward use of well understood two-point finite difference formulas, in particular when it comes to stabilization by proper upwinding. The theoretical understanding is advancing. An advantage is the possibility to prove

the conservation of qualitative properties like positivity, dissipativity, maximum principle in many cases for two- and three-dimensional problems independently of the mesh size.

For a significant class of geometries, mesh generators are available that can generate boundary conforming Delaunay meshes [84, 86], accompanied by active research [87].

There are a number of challenges connected with the use of the Voronoi finite volume method. It shifts a number of problems to mesh generation. In particular, the two-point flux approximation for the solution of anisotropic problems is convergent only under the condition that the discretization grids are aligned with the anisotropy direction [25]. There is no straightforward way to obtain higher order approximations. Therefore high accuracy solutions come with considerable costs.

Further directions include the convergence theory for further problem classes, see e.g. [27] for a first step for general nondegenerate reaction diffusion systems. The class of domains for which boundary conforming Delaunay meshing works still needs enlargement. Anisotropic boundary conforming Delaunay meshing for anisotropic problems as well as the resolution of boundary and interior layers is in its very infancy, i.e. corresponding proper meshes have to be "hand crafted" in many cases [33, 39].

References

[1] M. Acosta, C. Merten, G. Eigenberger, H. Class, R. Helmig, B. Thoben, and H. Müller-Steinhagen, Modeling non-isothermal two-phase multicomponent flow in the cathode of PEM fuel cells, *Journal of Power Sources* **159** (2006), 1123–1141.

[2] G. Allaire, A. Mikelić, and A. Piatnitski, Homogenization of the linearized ionic transport equations in rigid periodic porous media, *Journal of Mathematical Physics* **51** (2010), 123103–123103.

[3] D. Allen and R. Southwell, Relaxation methods applied to determine the motion, in two dimensions, of a viscous fluid past a fixed cylinder, *Quart. J. Mech. and Appl. Math.* **8** (1955), 129–145.

[4] P. Atkins and J. de Paula, *Atkins' Physical Chemistry*, W. H. Freman and Company, New York, 2006.

[5] R. Bank and D. Rose, Some Error Estimates for the Box Method, *SIAM Journal on Numerical Analysis* **24** (1987), 777–787.

[6] A. J. Bard and L. R. Faulkner, *Electrochemical methods: fundamentals and applications*, 2, Wiley New York, 1980.

[7] M. Z. Bazant, K. Thornton, and A. Ajdari, Diffuse-charge dynamics in electrochemical systems, *Physical review E* **70** (2004), 021506.

[8] J. Bear and Y. Bachmat, *Introduction to Modeling of Transport Phenomena in Porous Media*, Kluwer, Dordrecht, 1990.

[9] G. S. Beavers and D. D. Joseph, Boundary conditions at a naturally permeable wall, *J. Fluid Mech* **30** (1967), 197–207.

[10] J. Becker, R. Flückiger, M. Reum, F. N. Büchi, F. Marone, and M. Stampanoni, Determination of material properties of gas diffusion layers: experiments and simulations using phase contrast tomographic microscopy, *Journal of The Electrochemical Society* **156** (2009), B1175.

[11] P. M. Biesheuvel, Y. Fu, and M. Z. Bazant, Diffuse charge and Faradaic reactions in porous electrodes, *Physical Review E* **83** (2011), 061507.
[12] Y. Bourgault, Y. Coudière, and C. Pierre, Existence and uniqueness of the solution for the bidomain model used in cardiac electrophysiology, *Nonlinear analysis: Real world applications* **10** (2009), 458–482.
[13] H. C. Brinkman, A calculation of the viscous force exerted by a flowing fluid on a dense swarm of particles, *Applied Scientific Research* **1** (1949), 27–34.
[14] F. Ciucci and W. Lai, Derivation of Micro/Macro Lithium Battery Models from Homogenization, *Transport in Porous Media* **88** (2011), 249–270.
[15] F. Costantini, D. Gibson, M. Melcher, A. Schlosser, B. Spitzak, and M. Sweet, *FLTK 1.3*, http://fltk.org/doc-1.3/, 2011.
[16] Y. Coudière, C. Pierre, R. Turpault et al., Solving the fully coupled heart and torso problems of electro cardiology with a 3D discrete duality finite volume method, *submitted for publication* (2006).
[17] J. Divisek, J. Fuhrmann, K. Gärtner, and R. Jung, Performance Modeling of a Direct Methanol Fuel Cell, *J. Electrochem. Soc.* **150** (2003), A811–A825.
[18] M. Doyle, T. F. Fuller, and J. Newman, Modeling of galvanostatic charge and discharge of the lithium/polymer/insertion cell, *J. Electrochem Soc* **140** (1993), 1526–1533.
[19] W. Dreyer, C. Guhlke, and R. Müller, *Overcoming the shortcomings of the Nernst–Planck model*, *Phys. Chem. Chem. Phys.*, DOI: 10.1039/C3CP44390F, 2013.
[20] W. Dreyer, J. Jamnik, C. Guhlke, R. Huth, J. Moškon, and M. Gaberšček, The thermodynamic origin of hysteresis in insertion batteries, *Nature materials* **9** (2010), 448–453.
[21] A. Ern, R. Joubaud, and T. Lelievre, *Mathematical study of non-ideal electrostatic correlations in equilibrium electrolytes*, Nonlinearity **25**(2012), 1635
[22] J. Euler and W. Nonnenmacher, Stromverteilung in porösen Elektroden, *Electrochimica Acta* **2** (1960), 268–286.
[23] R. Eymard, J. Fuhrmann, and K. Gärtner, A Finite Volume Scheme for Nonlinear Parabolic Equations Derived from One-Dimensional Local Dirichlet Problems, *Numer. Math.* **102** (2006), 463–495.
[24] R. Eymard, J. Fuhrmann, and A. Linke, *MAC Schemes on Triangular Delaunay Meshes*, WIAS Berlin, Preprint no. 1654, 2011.
[25] R. Eymard, T. Gallouët, and R. Herbin, *The Finite Volume Method*, Handbook of Numer. Anal. (P. G. Ciarlet and J. L. Lions, eds.), VII, North-Holland, 2000, pp. 715–1022.
[26] W. Fang and K. Ito, Global solutions of the time-dependent drift-diffusion semiconductor equations, *J. Diff. Eq.* **123** (1995), 523–566.
[27] A. Fiebach, A. Glitzky and A. Linke, *Uniform global bounds for solutions of an implicit Voronoi finite volume method for reaction-diffusion problems*, WIAS Berlin, Preprint no. 1718, 2012.
[28] G. Flätgen and K. Krischer, A general model for pattern formation in electrode reactions, *The Journal of chemical physics* **103** (1995), 5428.
[29] P. C. Franzone and G. Savaré, Degenerate evolution systems modeling the cardiac electric field at micro-and macroscopic level, *Progress in nonlinear Differential Equations and Their Applications* **50** (2002), 49–78.
[30] P. Frolkovic, P. Knabner, C. Tapp, and K. Thiele, Adaptive finite volume discretization of density driven flows in porous media, *Transport de contaminants en milieux poreux (support de cours), CEA-EDF-INRIA, INRIA* (1997), 322–355.
[31] J. Fuhrmann, H. Zhao, E. Holzbecher, H. Langmach, M. Chojak, R. Halseid, Z. Jusys, and R. Behm, Experimental and numerical model study of the limiting current in a channel flow cell with a circular electrode, *Phys. Chem. Chem. Phys.* **10** (2008), 3784–3795.

[32] J. Fuhrmann, A. Linke, and H. Langmach, A numerical method for mass conservative coupling between fluid flow and solute transport, *Applied Numerical Mathematics* **61** (2011), 530–553.
[33] J. Fuhrmann, A. Linke, H. Langmach, and H. Baltruschat, Numerical calculation of the limiting current for a cylindrical thin layer flow cell, *Electrochimica Acta* **55** (2009), 430–438.
[34] H. Gajewski, On existence, uniqueness and asymptotic behavior of solutions of the basic equations for carrier transport in semiconductors, *ZAMM* **65** (1985), 101–108.
[35] H. Gajewski, On the uniqueness of solutions to the drift-diffusion model of semiconductor devices, *Math. Models Methods Appl. Sci* **4** (1994), 121–133.
[36] H. Gajewski and K. Gärtner, On the discretization of van Roosbroeck's equations with magnetic field, *Z. Angew. Math. Mech.* **76** (1996), 247–264.
[37] H. Gajewski and K. Gröger, Reaction - Diffusion Processes of Electrically Charged Species, *Math. Nachr.* **177** (1996), 109–130.
[38] T. Gallouët, R. Herbin, and M. H. Vignal, Error Estimates on the Approximate Finite Volume Solution of Convection Diffusion Equations with General Boundary Conditions, *SIAM J. Numer. Anal.* **37** (2000), 1935–1972.
[39] K. Gärtner and R. H. Richter, DEPFET sensor design using an experimental 3d device simulator, *Nucl. Instr. Meth. Phys. Res. A* **568** (2006), 12–17.
[40] H. H. Gerke and M. T. Van Genuchten, A dual-porosity model for simulating the preferential movement of water and solutes in structured porous media, *Water Resources Research* **29** (1993), 3054119.
[41] A. Glitzky and K. Gärtner, Energy estimates for continuous and discretized electro-reaction–diffusion systems, *Nonlinear Analysis: Theory, Methods & Applications* **70** (2009), 788–805.
[42] F. H. Harlow and J. E. Welch, Numerical calculation of time-dependent viscous incompressible flow of fluid with free surface, *Physics of fluids* **8** (1965), 2182–2189.
[43] R. Helmig et al., *Multiphase flow and transport processes in the subsurface: a contribution to the modeling of hydrosystems.*, Springer-Verlag, 1997.
[44] F. Hermeline, A finite volume method for the approximation of diffusion operators on distorted meshes, *Journal of computational Physics* **160** (2000), 481–499.
[45] U. Hornung, *Homogenization and porous media*, 6, Springer Verlag, 1997.
[46] R. Ierusalimschy and H. Figuredo, *Lua*, http://lua.org, 2012.
[47] A. M. Il'in, A difference scheme for a differential equation with a small parameter multiplying the second derivative, *Mat. Zametki* **6** (1969), 237–248.
[48] W. Jäger and A. Mikelić, On the interface boundary condition of Beavers, Joseph, and Saffman, *SIAM Journal on Applied Mathematics* (2000), 1111–1127.
[49] W. Krassowska and J. C. Neu, Effective boundary conditions for syncytial tissues, *Biomedical Engineering, IEEE Transactions on* **41** (1994), 143–150.
[50] A. Kraytsberg and Y. Ein-Eli, Review on Li–air batteries–Opportunities, limitations and perspective, *Journal of Power Sources* **196** (2011), 886–893.
[51] O. S. Ksenzhek and V. V. Stender, On the Distribution of Current in a Porous Electrode, in: *Dokl. Akad. Nauk SSSR*, 107, pp. 280–283, 1956.
[52] A. Kulikovsky, *Analytical Modeling of Fuel Cells*, Elsevier, 2010.
[53] K. Kumaresan, Y. Mikhaylik, and R. E. White, A mathematical model for a lithium–sulfur cell, *Journal of the Electrochemical Society* **155** (2008), A576.
[54] M. Landstorfer, S. Funken, and T. Jacob, An advanced model framework for solid electrolyte intercalation batteries, *Phys. Chem. Chem. Phys.* **13** (2011), 12817–12825.
[55] R. D. Lazarov, I. D. Mishev, and P. S. Vassilevski, Finite volume methods for convection-diffusion problems, *SIAM J. Numer. Anal.* **33** (1996), 31–55.
[56] M. Le Bars and M. Worster, Interfacial conditions between a pure fluid and a porous medium: implications for binary alloy solidification, *Journal of Fluid Mechanics* **550** (2006), 149–173.

[57] V. G. Levich, *Physicochemical Hydrodynamics*, Prentice-Hall, Englewood Cliffs, N. J, 1962.
[58] S. Litster, D. Sinton, and N. Djilali, Ex situ visualization of liquid water transport in PEM fuel cell gas diffusion layers, *Journal of Power Sources* **154** (2006), 95–105.
[59] T. S. Lundgren, Slow flow through stationary random beds and suspensions of spheres, *Journal of Fluid Mechanics* **51** (1972), 273–299.
[60] R. H. Macneal, An asymmetrical finite difference network, *Quart. Math. Appl.* **11** (1953), 295–310.
[61] M. Mangold, M. Krasnyk, and K. Sundmacher, Theoretical investigation of steady state multiplicities in solid oxide fuel cells*, *Journal of applied electrochemistry* **36** (2006), 265–275.
[62] S. Matera and K. Reuter, Transport limitations and bistability for in situ CO oxidation at RuO2(110): First-principles based multiscale modeling, *Phys. Rev. B* **82** (2010), 085446.
[63] C. Moyne and M. A. Murad, Electro-chemo-mechanical couplings in swelling clays derived from a micro/macro-homogenization procedure, *International journal of solids and structures* **39** (2002), 6159–6190.
[64] A. L. Muler and V. S. Markin, Electrical properties of anisotropic neuromuscular syncytia. I. Distribution of the electrotonic potential]., *Biofizika* **22** (1977), 307.
[65] M. A. Murad and C. Moyne, A dual-porosity model for ionic solute transport in expansive clays, *Computational Geosciences* **12** (2008), 47–82.
[66] J. C. Neu and W. Krassowska, Homogenization of syncytial tissues., *Critical reviews in biomedical engineering* **21** (1993), 137.
[67] J. Newman and K. Thomas-Alyea, *Electrochemical Systems*, Wiley-Interscience, 2004, 3rd Edition.
[68] J. Newman and W. Tiedemann, Porous-electrode theory with battery applications, *AIChE Journal* **21** (1975), 25–41.
[69] J. S. Newman and C. W. Tobias, Theoretical analysis of current distribution in porous electrodes, *Journal of the Electrochemical Society* **109** (1962), 1183.
[70] J. Nicolaides, T. A. Porsching, and C. A. Hall, *Covolume Methods in Computational Fluid dynamics*, Computation Fluid Dynamics Review (M. Hafez and K. Oshma, eds.), John Wiley and Sons, New York, 1995, pp. 279–299.
[71] N. Paust, C. Litterst, T. Metz, M. Eck, C. Ziegler, R. Zengerle, and P. Koltay, Capillary-driven pumping for passive degassing and fuel supply in direct methanol fuel cells, *Microfluidics and nanofluidics* **7** (2009), 531–543.
[72] M. Pennacchio, G. Savaré, and P. C. Franzone, Multiscale modeling for the bioelectric activity of the heart, *SIAM journal on mathematical analysis* **37** (2006), 1333.
[73] K. Promislow and B. Wetton, PEM fuel cells: a mathematical overview, *SIAM Journal on Applied Mathematics* **70** (2009), 369–409.
[74] N. Ray, A. Muntean, and P. Knabner, Rigorous homogenization of a Stokes–Nernst–Planck–Poisson system, *Journal of Mathematical Analysis and Applications* **390** (2012), 374–393.
[75] T. Roubíček, Incompressible ionized fluid mixtures, *Continuum Mechanics and Thermodynamics* **17** (2006), 493–509.
[76] I. Rubinstein, *Electro-diffusion of ions*, 11, Society for Industrial Mathematics, 1990.
[77] P. G. Saffman, On the boundary condition at the surface of a porous medium, *Stud. Appl. Math* **50** (1971), 93–101.
[78] D. L. Scharfetter and H. K. Gummel, Large signal analysis of a silicon Read diode, *IEEE Trans. Electron. Dev.* **16** (1969), 64–77.
[79] M. Schmuck, Analysis of the Navier-Stokes-Nernst-Planck-Poisson system, *Math. Models Meth. Appl. Sci* **19** (2009), 993.

[80] M. Schmuck and M. Z. Bazant, Homogenization of the Poisson–Nernst–Planck Equations for Ion Transport in Charged Porous Media, *Arxiv preprint arXiv:1202.1916* (2012).
[81] M. Schmuck and Berg P., Homogenization of a catalyst layer model for periodically distributed pore geometries in PEM fuel cells, *Arxiv preprint arXiv:1204.6699* (2012).
[82] B. Scrosati and J. Garche, Lithium batteries: Status, prospects and future, *Journal of Power Sources* **195** (2010), 2419–2430.
[83] J. R. Shewchuk, *Triangle: Engineering a 2D Quality Mesh Generator and Delaunay Triangulator*, Applied Computational Geometry: Towards Geometric Engineering (M. C. Lin and D. Manocha, eds.), Lect. Notes in Comput. Sci. 1148, Springer, 1996, pp. 203–222.
[84] J. R. Shewchuk, *Triangle*, http://www.cs.cmu.edu/~quake/triangle.html, 2006.
[85] Z. Shi and X. Wang, Comparison of Darcy´s Law, the Brinkman Equation, the Modified NS Equation and the Pure Diffusion Equation in PEM Fuel Cell Modeling, in: *Proceeding of the COMSOL Conference*, 2007.
[86] H. Si, *TetGen*, http://tetgen.org, 2012.
[87] H. Si and K. Gärtner, 3D boundary recovery by constrained Delaunay tetrahedralization, *International Journal for Numerical Methods in Engineering* **85** (2011), 1341–1364.
[88] H. Si, K. Gärtner, and J. Fuhrmann, Boundary conforming Delaunay mesh generation, *Comput. Math. Math. Phys.* **50** (2010), 38–53.
[89] T. Streckenbach, J. Fuhrmann, H. Langmach and M. Uhle, *pdelib*, http://pdelib.org, 2012.
[90] R. S. Varga, *Matrix iterative analysis*, Prentice-Hall, 1962.
[91] A. Z. Weber and J. Newman, Transport in polymer-electrolyte membranes, *Journal of the Electrochemical Society* **150** (2003), A1008.
[92] T. A. Zawodzinski, J. Davey, J. Valerio, and S. Gottesfeld, The water content dependence of electro-osmotic drag in proton-conducting polymer electrolytes, *Electrochimica Acta* **40** (1995), 297–302, Polymer electrolyte fuel cells.